

©2023 Society of Photo-Optical Instrumentation Engineers (SPIE). One print or electronic copy may be made for personal use only. Systematic reproduction and distribution, duplication of any material in this paper for a fee or for commercial purposes, or modification of the content of the paper are prohibited.

**Citation:**

Andrew Newton, Alex McCafferty-Leroux, S. Andrew Gadsden, Kevin R. Turpie, "Towards a second-generation robotic telescope mount for the airLUSI instrument," Proc. SPIE 12546, Sensors and Systems for Space Applications XVI, 125460J (13 June 2023); doi: 10.1117/12.2663887

**DOI:**

<https://doi.org/10.1117/12.2663887>

Access to this work was provided by the University of Maryland, Baltimore County (UMBC) ScholarWorks@UMBC digital repository on the Maryland Shared Open Access (MD-SOAR) platform.

**Please provide feedback**

Please support the ScholarWorks@UMBC repository by emailing scholarworks-group@umbc.edu and telling us what having access to this work means to you and why it's important to you. Thank you.

# PROCEEDINGS OF SPIE

[SPIDigitalLibrary.org/conference-proceedings-of-spie](https://SPIDigitalLibrary.org/conference-proceedings-of-spie)

## Towards a second-generation robotic telescope mount for the air-LUSI instrument

Andrew Newton, Alex McCafferty-Leroux, S. Andrew Gadsden, Kevin Turpie

Andrew Newton, Alex McCafferty-Leroux, S. Andrew Gadsden, Kevin R. Turpie, "Towards a second-generation robotic telescope mount for the air-LUSI instrument," Proc. SPIE 12546, Sensors and Systems for Space Applications XVI, 125460J (13 June 2023); doi: 10.1117/12.2663887

**SPIE.**

Event: SPIE Defense + Commercial Sensing, 2023, Orlando, Florida, United States

# Towards a Second-Generation Robotic Telescope Mount for the air-LUSI Instrument

Andrew Newton<sup>a</sup>, Alex McCafferty-Leroux<sup>a</sup>, S. Andrew Gadsden<sup>a</sup>, and Kevin R. Turpie<sup>b</sup>

<sup>a</sup>McMaster University, ON L8S 4L7, Canada

<sup>b</sup>University of Maryland, Baltimore County, MD 21250, United States of America

## ABSTRACT

Earth observation satellites, such as those responsible for monitoring the effects of climate change, require rigorous calibration protocols to account for on-orbit sensor degradation. An increasingly dependable method to address this issue uses the Moon as a reference light source for in-situ calibration. The airborne lunar spectral irradiance (air-LUSI) mission aims to improve the utility of the Moon as an on-orbit calibration target for remote sensing instruments, by tying the currently accepted lunar model to the SI and establishing lunar irradiance on an absolute scale. To this end, air-LUSI collects SI-traceable measurements of lunar irradiance at visible to near-infrared wavelengths with unprecedented accuracy. A non-imaging telescope is flown at an altitude of 21 km, aboard NASA's high-altitude ER-2 aircraft, which places the instrument above 95% of the Earth's atmosphere for clean, minimally obstructed lunar spectra. To fix the optical axis on the Moon during flight, an autonomous control system is required to compensate for aircraft motion and track the Moon across its celestial transit. In this paper, we present an overview of the robotic subsystem used to track the Moon on more than ten high-altitude flights, and the valuable lessons learned from those campaigns. From this insight, a preliminary design for a second-generation robotic telescope mount is presented. Referred to as the HAAMR, it will supplant the current robotics system on future air-LUSI Operational Flight Campaigns, with the nearest field deployment slated for January 2024. We show how this new system is poised to offer a more reliable, accurate, and responsive platform for the air-LUSI instrument to continue collecting data that will ultimately help to improve our understanding of the Earth's climate.

**Keywords:** target tracking, computer vision, robotics, lunar calibration

## 1. INTRODUCTION

The airborne LUnar Spectral Irradiance (air-LUSI) instrument is one important thrust in the broader initiative of establishing the Moon as an SI-traceable, on-orbit calibration source for remote sensing instruments, such as those of NASA's Earth Observing System (EOS), for example. The primary function of the EOS is to acquire long-term global observations of the Earth's many climate variables, some of which include atmospheric composition, ocean color, ocean temperature, as well as various surface features (vegetation, snow cover, sea ice). Essentially, the EOS aims to generate the required data sets for a comprehensive understanding of the Earth's climate. However, measuring these important climate variables is anything but trivial – the measurements must be accurate and stable. For instance, it's been determined that remote sensing instruments must be capable of detecting temperature trends as low as  $0.1^\circ$  deg/decade, ozone variations as little as 1%/decade, all the while maintaining measurement stability of 1% over a decade.<sup>1</sup>

The harsh environment of space offers further complexities. The responsivity of remote imaging sensors departs from their pre-launch calibrations over time, a consequence in part of thermal cycling and adverse radiation effects. Historically, celestial bodies such as the Moon, the Sun, and some particular sites on the Earth have been used to trend a spacecraft sensor's temporal degradation – a relative calibration technique. Although relative calibration can satisfy the measurement stability requirement specified by NIST7047, demonstrated by

---

Further author information: (Send correspondence to A.N. or S.A.G.)

A.N.: E-mail: newtoa4@mcmaster.ca

S.A.G.: E-mail: gadsden@mcmaster.ca

Sensors and Systems for Space Applications XVI, edited by Genshe Chen,  
Khanh D. Pham, Proc. of SPIE Vol. 12546, 125460J · © 2023 SPIE  
0277-786X · doi: 10.1117/12.2663887

Proc. of SPIE Vol. 12546 125460J-1

the SeaWiFS spacecraft,<sup>2</sup> the fact that many other climate variable accuracy metrics are tied to the SI requires that a remote sensing instrument is also calibrated to the SI in an absolute sense.

Accordingly, there is a recognized need in the satellite instrument calibration community for an on-orbit, absolute, SI-traceable calibration target to meet the accuracy and stability demands of current, future (and past) Earth observation missions. The Moon was identified as an ideal candidate for this role for a number of radiometric benefits, with the incredible stability in its surface reflectance, estimated at one part in  $10^8$  per year,<sup>3</sup> as the most compelling radiometric feature. However, there are also a number of challenges in establishing the Moon as a calibration light source, namely the non-uniformity of lunar surface albedo, brightness variations resulting from lunar phase and libration, and the strong dependence on the Sun-Moon-Observers geometry.<sup>4</sup> The complex interdependency of these factors requires that a lunar irradiance model, taking a particular lunar illumination and observation geometry as input and providing lunar irradiance as output, is available for spacecraft to confirm their measurements against.

The United States Geological Survey (USGS) has developed and continues to maintain the currently accepted lunar calibration model,<sup>5</sup> referred to as the RObotic Lunar Observatory (ROLO) model. Observational data used to build the ROLO model was acquired from a ground-based facility in Flagstaff, Arizona, and thus required correction factors for atmospheric effects (absorption, scattering, etc) and other sources of measurement corruption. These corrections introduce uncertainty into the measurements, and as a result, the ROLO model cannot demonstrate absolute uncertainties below 5%, with up to 4% owing to atmospheric effects.<sup>6</sup>

The air-LUSI instrument was developed to circumvent the issue of atmospheric corruption. Stationed in the wing pod of a NASA ER-2 aircraft, a repurposed U2 spy plane pictured below in Fig. 1, air-LUSI acquires lunar spectra through a windowless zenith viewport at an altitude of 21 km (70 000 ft).<sup>7</sup> From this vantage point, the instrument makes highly accurate, SI-traceable measurements above 95% of the Earth's atmosphere. In doing so, the air-LUSI program seeks to improve the Moon's utility as an absolute calibration target, by reducing the absolute uncertainties in the ROLO model and tying lunar irradiance measurements to the SI.



Figure 1: NASA's Earth Resources (ER-2) aircraft. The wing pods protrude fore and aft from the relatively massive wings. The zenith viewport is located on the aft-body of the starboard side wing pod. Credits: NASA/Jim Ross.

Air-LUSI is comprised of three subsystems; the IRradiance Instrument Subsystem (IRIS), responsible for lunar spectra acquisition; the Autonomous Robotic Telescope Mount Instrument Subsystem (ARTEMIS)\*, which keeps the telescope fixed on the Moon during flight; and the High-altitude ER-2 Adaptation subsystem (HERA), which helps to protect thermally sensitive components from the extreme cold at altitude. Consider the figure below, which illustrates the layout of air-LUSI within the ER-2 wing pod.

\*named prior to the announcement of NASA's Artemis program in 2019, but for many of the same reasons.



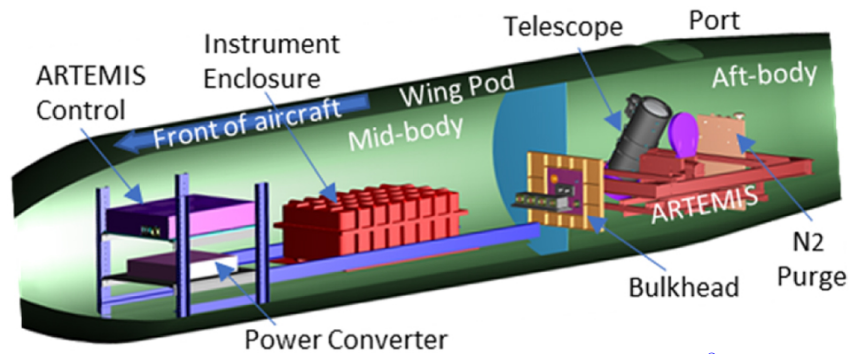


Figure 2: air-LUSI layout in the ER-2 wing pod.<sup>8</sup>

The mid-body has partial environmental control, which can maintain a minimum temperature and pressure of 0° C and 33.7 kPa (1/3 atm), respectively. The control electronics and the instrument enclosure are housed in this portion of the wing pod to protect against harsh atmospheric conditions. The aft-body is open to the atmosphere, where temperatures can easily plummet to −70° C and the ambient pressure is roughly 6.1 kPa (1/15 atm). The telescope and robotic control system are stationed here, which allows the telescope to acquire measurements through the windowless zenith viewport. A nitrogen purging system prevents condensation build-up inside the telescope by flushing the internal chamber during ascent and descent with inert gas.

To date, air-LUSI has completed more than ten high-altitude flights, collecting some of the most accurate lunar spectral measurements ever recorded. It's been estimated that air-LUSI has measured lunar irradiance with a combined standard uncertainty of 1% ( $k = 1$ ), and has established a path towards achieving uncertainties of 0.6%.<sup>9</sup> Obtaining this level of accuracy requires a series of rigorous pre- and post-flight calibration protocols, but ultimately depends on the ability of the telescope to stay locked on the Moon, regardless of aircraft or lunar motion. The IRIS telescope's particular design requires that the Moon remains within 0.5° of the optical axis<sup>8</sup> – this condition is the primary constraint and objective of the robotics subsystem.

The remainder of this work details the performance of the air-LUSI robotics subsystem, as well as the motivation and necessity of pursuing a robotics overhaul effort. First, we present an overview of the original system, named ARTEMIS, and its track record of mostly successful lunar tracking performance. Major lessons learned from the field campaigns are shared, which lay the foundation for the proposed upgrades. Next, we illustrate in the context of experimental data how the second-generation robotics design, named HAAMR, will improve lunar tracking dynamics and satisfy the desired changes.

## 2. PAST WORK AND MOTIVATION

### 2.1 ARTEMIS

The Autonomous Robotic Telescope Mount Instrument Subsystem (ARTEMIS) was originally commissioned as a Master's project in the Intelligent and Cognitive Engineering (ICE) Lab at the University of Guelph.<sup>10</sup> The complexity of developing this mission-critical system required the establishment of numerous design constraints, which are categorized below in Table 1. In summary, a corrosion-resistant airworthy telescope mount, with at minimum two degrees of freedom (DOFs), designed according to an extremely conservative margin of safety and employing a Computer Vision (CV) based feedback control system is required for the mission. Additionally, the system must integrate with an AFRC-provided mounting rack and operate within the narrow confines of the ER-2 aft-body wing pod, shown in Fig. 5. Paramount to all else, is the 0.5° tracking metric required for crisp lunar measurements. A rendering of the final ARTEMIS design is provided in Fig. 3.

The supporting structure of ARTEMIS is constructed from Aluminum 6061-T6, with stainless steel taking up the remainder of the components. A double gimbal mechanism with offset rotational axes provides the necessary DOFs and was intended to maximize the telescope's field of regard. Two Ultra Motion® Servo Cylinders (PNs: A2V9B-B0M3E2 and A2V9A-B0M3E2) independently control the azimuth and elevation angles of the telescope. Telemetry is received from the actuators through a serial interface, which can pass actuator data

air-LUSI Robotics Subsystem Constraints	
Geometric	<ul style="list-style-type: none"> <li>• Minimum <math>\pm 5^\circ</math> azimuthal range of motion.</li> <li>• Minimum <math>40^\circ - 77^\circ</math> elevation range of motion.</li> <li>• Must manipulate the telescope within the confines of the aft-body wing pod without any mechanical interference or field of view clipping.</li> <li>• The design should maximize the telescope's field of regard through the viewport.</li> </ul>
Autonomy	<ul style="list-style-type: none"> <li>• Keep the Moon within <math>0.5^\circ</math> of the telescope's Line of Sight (LOS).</li> <li>• Employ a closed-loop control system, using computer vision for target acquisition and state feedback.</li> <li>• Capable of entirely autonomous operation for a 45-minute tracking window.</li> <li>• The system must act as a Child to the Parent system IRIS, which toggles the state of the robot according to pilot switches activated from the cockpit.</li> <li>• The system must record high-frequency time-tagged data from the actuators, inertial measurement unit, and tracking camera.</li> </ul>
Airworthiness	<ul style="list-style-type: none"> <li>• The structure must be designed to yield in a crash loading scenario, representing load factors of <math>9g</math>, <math>3g</math>, and <math>4.5g</math> in the earthbound, fore, and starboard directions respectively.</li> <li>• Only aerospace-grade materials accompanied by Mill Test Reports are approved for instrument construction.</li> <li>• Only fasteners with accompanying Military Specification Certificates are approved for instrument construction.</li> <li>• All blind holes must include locking HeliCoil inserts to prevent bolt loosening.</li> </ul>
Environmental	<ul style="list-style-type: none"> <li>• Tolerate temperatures as low as <math>-70^\circ\text{C}</math>.</li> <li>• Withstand repeated wet-dry cycles from condensation during passage through high-humidity atmospheric zones.</li> </ul>

Table 1: air-LUSI robotics' autonomy, airworthiness, geometric, and environmental constraints.

such as temperature, position, and torque, at more than 250 Hz. Kamatics journal bearings with proprietary Karon™ self-lubricating liner are used to permit motion in the azimuth and elevation joints. A Basler (PN: acA1920-40um) monochromatic machine vision camera equipped with a Kowa Lens (PN: LM6HC) satisfies the CV feedback constraint with up to 41 fps of lunar position images. Autonomy is managed through a Robot Operating System (ROS) framework implemented on an Intel® NUC Kit (PN: NUC7i7BNHX1), located in the control electronics box of the mid-body compartment, running Ubuntu 16.04 with the ROS Lunar Loggerhead distribution. A thorough account of the ARTEMIS' mechanical and control system design is available in.<sup>10</sup>

## 2.2 Airborne Science Field Campaigns

Spanning from August 2018 to March 2022, ARTEMIS has since embarked on more than 10 high-altitude flights across three field campaigns out of NASA's Armstrong Flight Research Center (AFRC) in Palmdale, California. Air-LUSI flights usually occur after midnight (local time PST/PDT), and must be scheduled months in advance to pinpoint the specific timeframes when the Moon occupies viewable elevation angles from the wing pod (greater

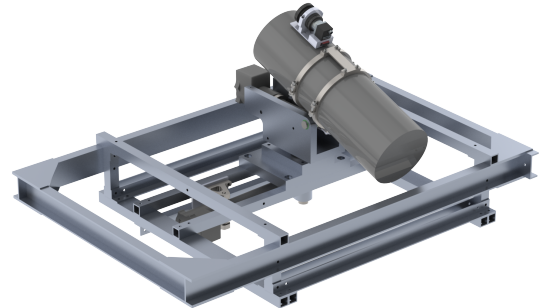
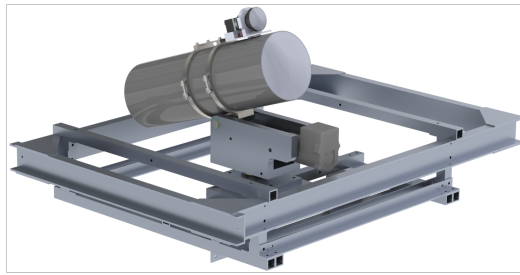


Figure 3: The ARTEMIS system.

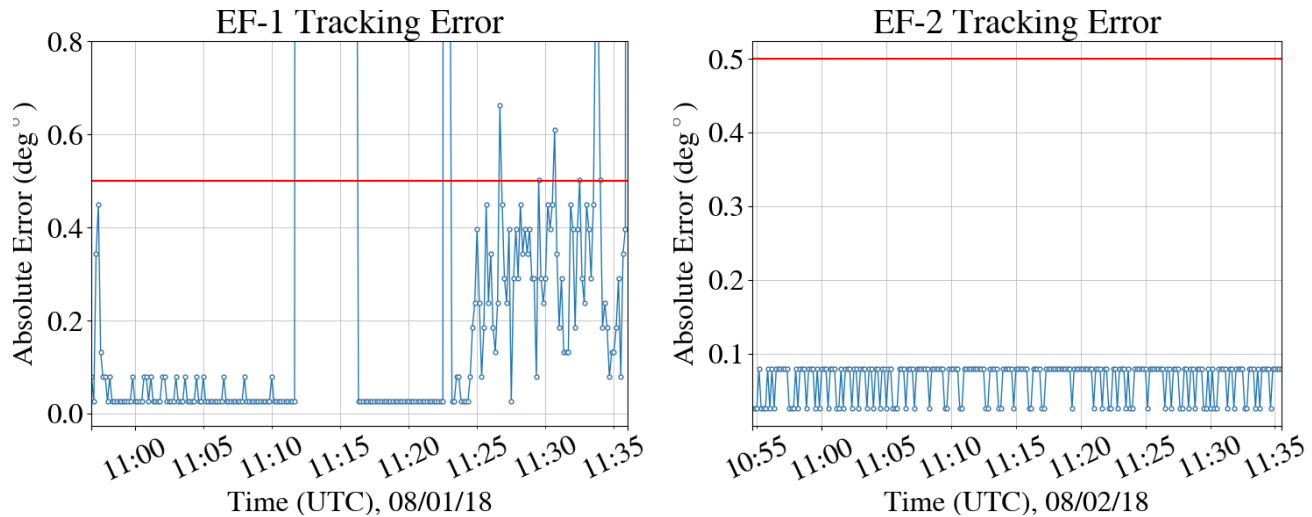


Figure 4: Target tracking performance from the Engineering Flight Campaign.

than  $45^\circ$  above horizontal) and the lunar phase angle coincides with observational requirements dictated by USGS and NIST.

The tracking performance of ARTEMIS is evaluated by the pixel offset in the CV camera frame between a predetermined pixel setpoint (that which aligns the Moon with the center of the telescope) and the center of the Moon. It was experimentally determined that the particular camera/lens combination provides  $0.053^\circ$  of angular resolution per pixel.<sup>10</sup> The absolute pixel offset, obtained from the squared sum of squares of  $x$  and  $y$  pixel offsets, is then converted to an angular displacement for comparison with the  $0.5^\circ$  mission constraint. Pixel error data is recorded at the control loop rate of 30 Hz. For the presentation of tracking performance over a 40-minute window, the data is downsampled to 0.1 Hz (10 second bins), using the mean of the data over the bin as the reported value. This method provides a good understanding of the system's performance as a whole, but masks off-target excursions that may have occurred rapidly. Full-resolution tracking error plots are provided in Appendix A.

### 2.2.1 Engineering Flight Campaign

The first airborne test of ARTEMIS was the Engineering Flight Campaign (EFC) in August 2018. The purpose of the EFC was to validate the airworthiness of the various instrument subsystems, ensure proper integration with the ER-2, and confirm instrument control via the cockpit pilot switches. The EFC consisted of two flights occurring on August 1st and 2nd 2018, denoted EF-1 and EF-2. The moon occupied elevation angles from  $50^\circ$ - $55^\circ$  above the horizon, placing the moon just slightly above the bottom edge of the viewport. The plots in Fig. 4 depict the target tracking performance for the EFC.

Figure 4 confirms that the EFC was largely a success for the robotics subsystem. However, a hard drive failure on the IRIS computer occurred nearly 15 minutes into EF-1, requiring a full air-LUSI power cycle. This is why the tracking error departs off the chart at 11:10, as ARTEMIS returns the telescope to its stowed position. The

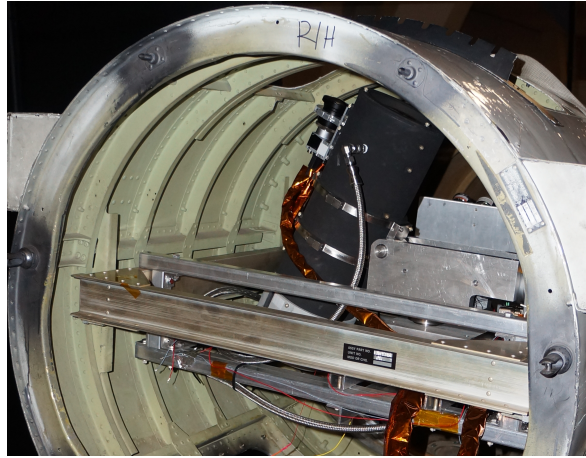


Figure 5: Required configuration of ARTEMIS for installation in the wing pod aft-body. Credit: Kevin Turpie/UMBC.

system restart unfortunately did not fix the failed drive, as evidenced by unacceptable tracking results for the remainder of EF-1, because IRIS was incapable of sending the child system ARTEMIS into tracking mode. As a result, the telescope remained stationary at the initial tracking condition. The failed hard drive was replaced for EF-2, which thankfully saw great success as the telescope was locked on its target for the entire tracking window.

Integration with the ER-2 was narrowly approved, as it was discovered that the telescope interfered with the wing pod during installation when in the stowed position. Luckily, moving the telescope to its initial tracking condition, at an elevation angle of  $70^\circ$ , cleared the interference and allowed for instrument upload as shown in Fig. 5.

Although the tracking results of the EFC were rightfully celebrated by the air-LUSI team, some troubling problems were encountered upon return to the NIST laboratory. The intention was to leverage the autonomous capabilities of ARTEMIS to alleviate some tedious calibration efforts, but when operating at room temperature for extended periods of time, the elevation actuator overheated and completely fried the internal motherboard. This wasn't a problem operationally because of the frigid environment at altitude that served to draw heat from the actuator as a function of the difference between source and sink temperatures each raised to the fourth (radiative cooling, minimal convective or conductive heat transfer). Thankfully, the actuator was equipped with a self-locking acme screw and thus maintained the telescope's position even with a loss of power. If the actuator was of the ball-screw series offered by Ultra Motion<sup>®</sup>, the telescope would have fallen about the elevation axis and crashed into the frame, likely resulting in irreparable damage.

In an effort to keep flight software modifications minimal, the robotics team proposed a minor firmware change that switched the actuators from "Absolute Position Mode" to "Trajectory Generated Position Mode" – the former using the actuator's full power rating to achieve a given stroke setpoint, the latter constructing a trajectory generated motion according to preset acceleration and maximum velocity parameters. The ability to limit the acceleration limited the force, which reduced the current in the motor coils and thus the heat generation. Laboratory tests confirmed that the modification was effective in abating heat production and resulted in safe, steady-state motherboard temperature levels.

## 2.2.2 Demonstration Flight Campaign

ARTEMIS' second deployment was for the Demonstration Flight Campaign (DFC) in November 2019. In addition to re-confirming compatibility with the aircraft, the DFC aimed to prove that the instrument is indeed capable of achieving its intended scientific goals, namely, the acquisition of lunar spectral irradiance with sub-1% measurement uncertainty. From the perspective of the robotics team, however, the fundamental requirements of ARTEMIS were unchanged. The DFC consisted of five flights (denoted DF-1 through DF-5), occurring between November 12th and 17th 2019. Lunar elevations spanned the  $61^\circ$ - $71^\circ$  angle space, a marked increase from the

Engineering Flights. The plots in Fig. 6 chart the worst and best tracking results of the five total flights the campaign.

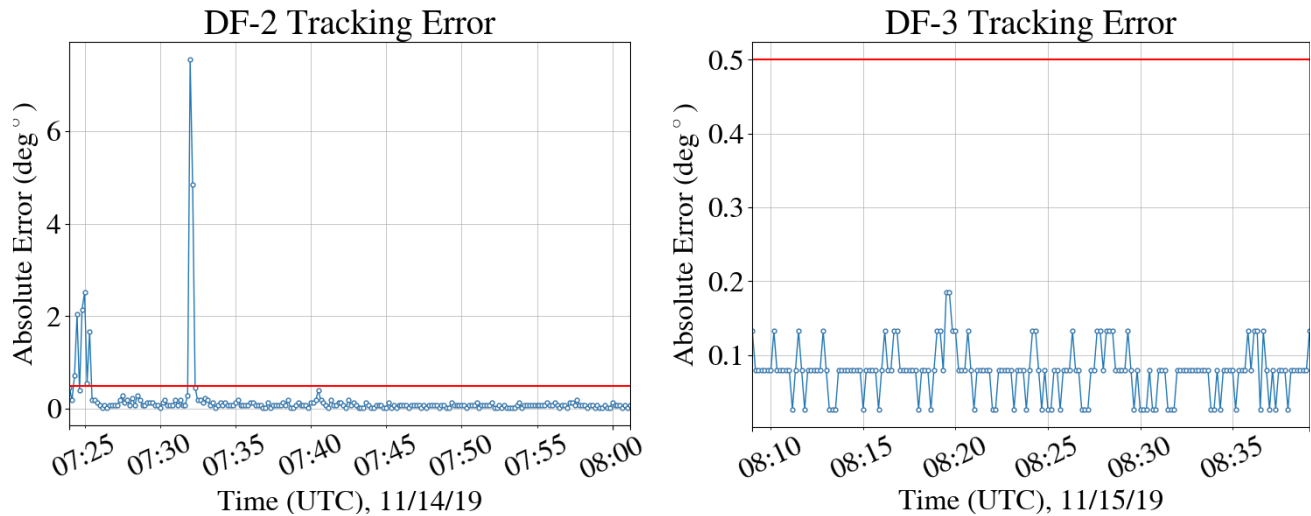


Figure 6: Worst and best target tracking performance plots from the Demonstration Flight Campaign.

The DFC was also a huge success, for both the robotics and the science team, but most importantly the instrument's ability to reach its intended scientific goals was confirmed.<sup>9</sup> The actuator firmware change following the EFC was effective against overheating in a laboratory setting but resulted in slightly looser tracking performance, as seen on DF-3. Although the mission constraint was still satisfied, this loss of performance from EF-2 was disconcerting. For the first 10 minutes of DF-2, the aircraft was exhibiting abnormal attitude dynamics as the pilot had accidentally increased the autopilot's yaw control gain, which activated a phugoid-like flight mode. Once the pilot had corrected the control gain, ARTEMIS tracked the Moon within the mission spec. Telemetry was also expanded from the EFC, with variables such as actuator torque and temperature being recorded at the control loop frequency. A full report of the DFC is provided in.<sup>11</sup>

### 2.2.3 Operational Flight Campaign 01

After more than two years of dormancy thanks to the global pandemic, ARTEMIS was most recently deployed on the Operational Flight Campaign 01 (OFC) in March 2022. After confirming the instrument could acquire lunar spectra with unprecedented accuracy, the air-LUSI instrument obtained its first operational dataset over four Operational Flights (OF-1 through OF-5) between March 13th and 17th 2022, with OF-2 canceled due to strong winds. Lunar elevations were similar to the DFC, from 57°-71°. Again, the best and worst of the tracking performance results are shown below in Fig. 7, with full resolution plots provided in Appendix A.

Although the tracking performance plots in Fig. 7 tell a similar story as the EFC and DFC, the OFC was anything but smooth sailing. From early on in the campaign, the team was met with a myriad of issues – component misalignment, elevation axis binding, cable snagging, range of motion reduction, as well as actuator overheating and risk of complete actuator failure. The team implemented a number of modifications to flight software, a risky last-resort action aimed at protecting the actuator from failure in flight and in the calibration lab. The primary fix was an actuator watchdog implemented in the main control loop that supervised the amount of current drawn by the actuator, rather than the temperature read by the motherboard sensor. Since the thermal time constant of the motor coils is far less than the temperature sensor on the motherboard, it's possible for the insulation on the motor coil windings to melt, thus creating a short circuit, before the temperature sensor reports a dangerous value. The watchdog would trip a latching error mode if the current draw was above a given threshold for more than 3 seconds. The error mode completely disabled the actuator, which afterward could only be recovered manually with a power cycle. The robotics team then had to also design and test a manual recovery protocol that could be used in flight should the error mode be tripped.



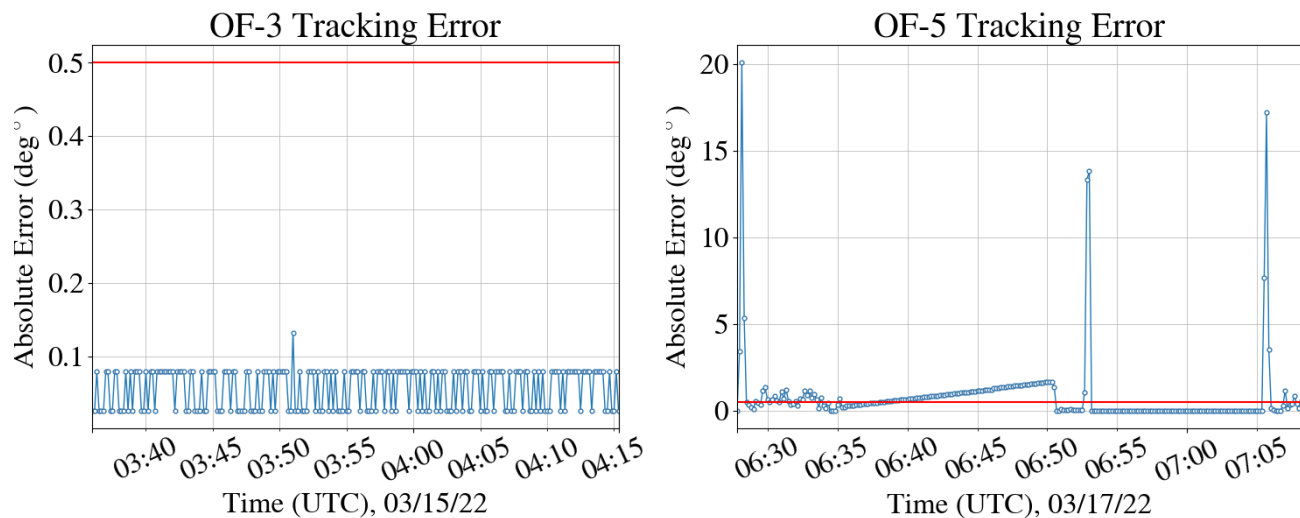


Figure 7: Best and worst target tracking performance results from the Operational Flight Campaign.

After three mostly successful flights, and one scrubbed flight due to high winds, the ARTEMIS was met with its most difficult test to date on OF-5. For the first 10 minutes of OF-5, the aircraft was experiencing aberrative levels of turbulence which ARTEMIS was not capable of correcting for. The increased inertial torques on the joints of ARTEMIS resulted in the first actuator failure at 06:35 UTC. The robotics team responded immediately with the first manual recovery sequence, jumping through a series of SSH connections to remotely access the ARTEMIS computer and initiate a power cycle. The instrument was recovered 15 minutes later at 06:50 UTC, at which point the turbulence had subsided and the telescope was locked on its target until 07:05 UTC. Beyond 07:05 UTC, turbulence had returned and caused a second and third actuator failure. The second failure was corrected in the same manner as the first, but after the third actuator failure the team agreed to abort the flight with the hope of having acquired enough usable data between the first and second failures. Thankfully this was the case, but following OF-5 it became clear to the team that major revisions, beyond simple software patches, would be required to continue deploying this instrument in a reliable manner.

### 3. PROPOSED DESIGN MODIFICATIONS

Following the OFC, the air-LUSI team identified several key changes to the robotics system that would serve to eliminate sources of risk and improve lunar tracking performance. The new design's primary goals are to reduce the loads on the linear actuators, increase the telescope's field of regard, and improve high-frequency disturbance rejection during turbulence. The overarching goal of this design challenge is to modify the mechanics of how the telescope is manipulated – the operational characteristics (i.e. the child/parent architecture of ARTEMIS/IRIS systems, electrical integration with the aircraft) and the calibration routine will remain untouched. The competing designs are illustrated in Fig. 8.

#### 3.1 Reducing Actuator Loads

There are a number of factors that contributed to actuator burnout. First, the completed telescope weighed in at a total of 35 lbs, more than double the initial estimate of 15 lbs. This is undesirable for several reasons, but most pertinent to the robotics was the narrowing of the control input margin of safety. The increased weight was exacerbated by the awkward gimbal configuration with offset axes, which not only limits the available joint torque due to restrictive transmission link geometries, but also introduces gravitational torque about the joint axes as a nonlinear function of the manipulator's configuration. Even though the actuators can each provide 70 lbs of continuous thrust without overheating, the eccentricity of the telescope's Center of Gravity (CG) about the elevation axis requires the actuator to operate beyond its safe regime and thus generate more heat than it can dissipate. From a mechanical design perspective, it follows that the primary cause of actuator burnout was the unexpectedly high level of gravitational torque produced by the offset telescope. It is clear that the bisecting

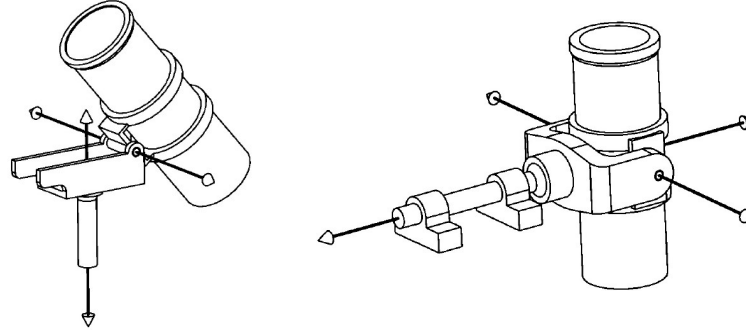


Figure 8: The offset axes (left) and bisecting axes (right) design alternatives.

axes alternative would offer a significant reduction in the gravitational torque if the intersection point of the two axes, the Center of Rotation (CR), is located as near to the CG as possible. In an ideal system, the CG would be coincident with the CR, in which case gravitational torque would drop out of the equations of motion entirely and the actuators would only need to overcome rotational inertia. Practically, the CG to CR distance can be designed such that the moment arm created by the CG is less than the moment arm for the actuator, which would restore the control input margin of safety.

### 3.2 Field of Regard

Field of Regard (FOR) refers to the total viewable area for a given sensor's LOS. For a mobile sensor, such as the IRIS telescope mounted on a double gimbal manipulator, the FOR is a function of the manipulator's range of motion for each DOF. In the following analysis, the forward kinematics method based on the modified Denavit-Hartenberg (DH) convention<sup>12</sup> is used to plot the reachable worksurface of the telescope lens' center point, which represents the origin of the LOS. The FOR is then understood as the area defined by the normal projection of this surface's edges through the wing pod's viewport. □ Consider Fig. 9, which illustrates ARTEMIS' Forward Kinematics Model (FKM) with the associated DH parameters defined in Table 2. The origin of the base frame 0 (denoted {0}), is concentric with the wing pod tube and located on a plane centered in the width of the viewport. The  $x$ -axis of frame 4 (denoted {4}), represents the telescope's LOS. {1} through {3} define the rigid bodies in the kinematic chain.  $q_1(t)$  and  $q_3(t)$  are the azimuth and elevation joint variables respectively, and  $L_1$  through  $L_6$  define the geometry of the manipulator. The FKM takes as input the vector of joint angles,  $\mathbf{q} = [q_1, q_3]$ , and returns the position and orientation (pose) of the last frame in the kinematic chain with respect to the base frame. The LOS frame's pose is described by the homogeneous Transformation Matrix (TM) which defines {4} relative to the base {0} as,

$${}^0_4T = {}^0_1T {}^1_2T {}^2_3T {}^3_4T = \left[ \begin{array}{c|c} {}^0_4R & {}^0P_4 \\ \hline 0 & 1 \end{array} \right], \quad (1)$$

in which  ${}^0_4R \in \mathbb{R}^{3 \times 3}$  is a rotation matrix describing the orientation of {4} wrt {0}, and  ${}^0P_4 \in \mathbb{R}^{3 \times 1}$  relates the position of {4} origin relative to {0}. The TM for neighbouring frames in the kinematic chain,  ${}^{i-1}_iT$  is given by

$${}^{i-1}_iT = \begin{bmatrix} c\theta_i & -s\theta_i & 0 & a_{i-1} \\ s\theta_i c\alpha_{i-1} & c\theta_i c\alpha_{i-1} & -s\alpha_{i-1} & -s\alpha_{i-1}d_i \\ s\theta_i s\alpha_{i-1} & c\theta_i s\alpha_{i-1} & c\alpha_{i-1} & c\alpha_{i-1}d_i \\ 0 & 0 & 0 & 1 \end{bmatrix}. \quad (2)$$

The reachable worksurface of the LOS origin for the offset axes design is plotted in Fig. 10, in which the blue surface contains all possible values for  ${}^0P_4$ , the grey surface is the viewport opening, the black dyads represent the frames of Fig. 9, and green lines depict link offset parameters  $L_1$  through  $L_6$ , which were obtained from a CAD model of the manipulator.



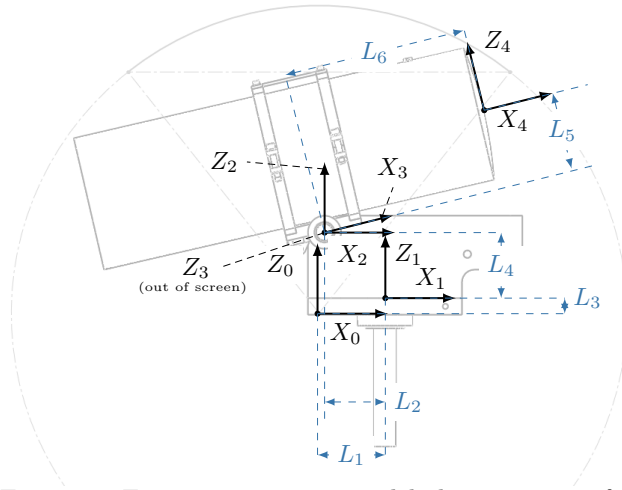


Figure 9: Frame assignments and link parameters for the ARTEMIS manipulator.

$i$	$\alpha_{i-1}$	$a_{i-1}$	$d_i$	$\theta_i$
1	0	$L_1$	$L_3$	$q_1(t)$
2	0	$-L_2$	$L_4$	0
3	$\pi/2$	0	0	$q_3(t)$
4	$\pi/2$	$L_6$	$L_5$	0

Table 2: DH Parameters for ARTEMIS.

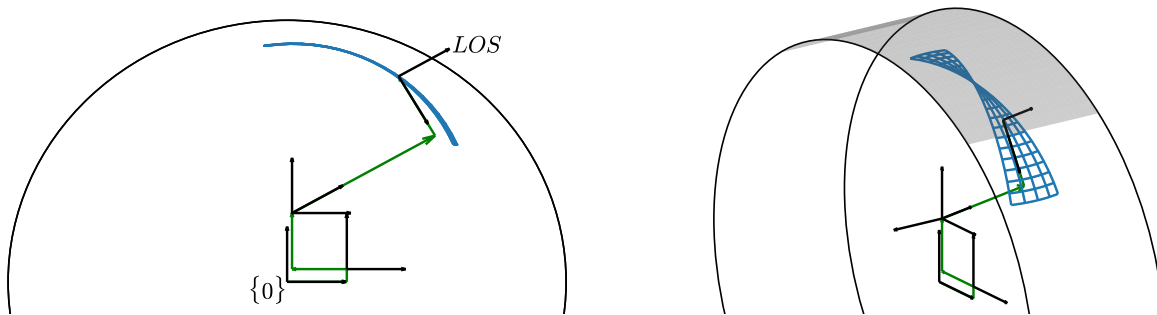


Figure 10: Illustration of the reachable workspace for the offset axes design.

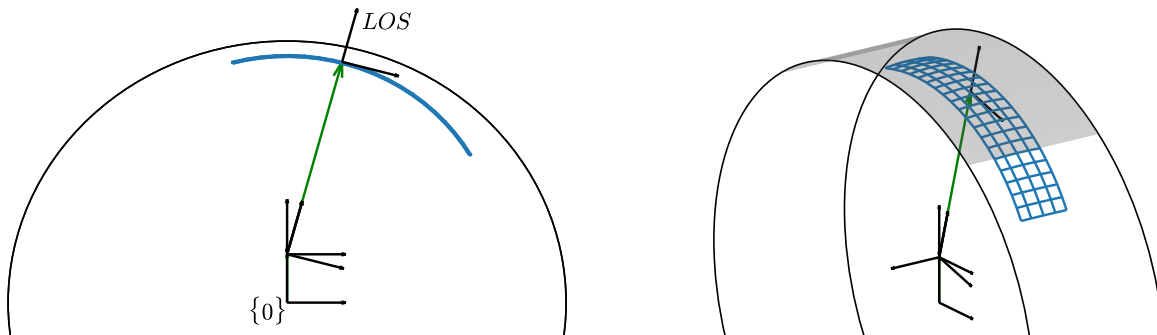


Figure 11: Illustration of the reachable workspace for the bisecting axes design.

Consider now the bisecting axes alternative, for which the workspace is much easier to imagine because the LOS intersects the CR. Thus, the LOS origin point would trace out a spherical surface whose radius is equal to the distance from that point to the CR. The extremities of the spherical surface would be defined by each DOFs particular range of motion. This intuitive result is confirmed by Fig. 11. It is clear from the reachable workspace plots that the bisecting axis alternative would offer a larger FOR over the offset axes design, in addition to the loading benefits described prior in Section 3.1

### 3.3 Improved Aircraft Disturbance Rejection

The current gimbal configuration of the offset axes design aligns the azimuth and elevation joints with the aircraft's yaw and roll axes, respectively. Interestingly, the pitch axis of the ER-2 is the most dynamic, a source of disturbance for which there is no direct control input. Consider the plots below in Figs. 12 and 13, which illustrate the relationship of the azimuthal and elevation errors ( $x$  and  $y$  pixel errors) with the pitch and roll attitude dynamics, respectively. Normalized values are charted in these plots in order to detect temporal relationships between the various signals.

Figure 12 indicates a strong dependence of the azimuthal error on the pitch attitude dynamics, especially during rapid attitude motion as indicated by the slope of the pitch signal. This indicates that the azimuth controller, one of two decoupled controllers in this system, is ineffective in correcting for rapid pitch movements. Given that a normalized value of 0.8 for the azimuth error signal corresponds with a zero pixel offset, it is evident that the azimuth controller can slightly maintain target tracking during slow pitch attitude dynamics, as seen between 07:06:07 and 07:06:45 UTC.

Figure 13 shows a similar affinity between the elevation error signal and the roll attitude dynamics. Although, the relationship is far less pronounced because the roll attitude dynamics are less severe, and the elevation controller has a direct control input to this form of disturbance which results in better target tracking on this axis – a normalized value of 0.3 corresponds to zero pixel offset for the elevation error signal.

The results of this section serve to further support the bisecting axes design alternative. The gimbal axes can easily be aligned with the pitch and roll axes of the aircraft, which would offer improved control authority as per the results of Fig. 13.

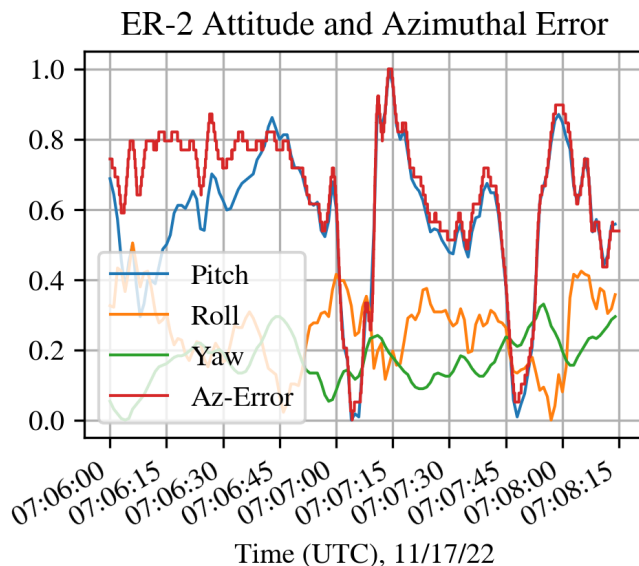


Figure 12: Azimuthal error dependence on the pitch attitude dynamics.

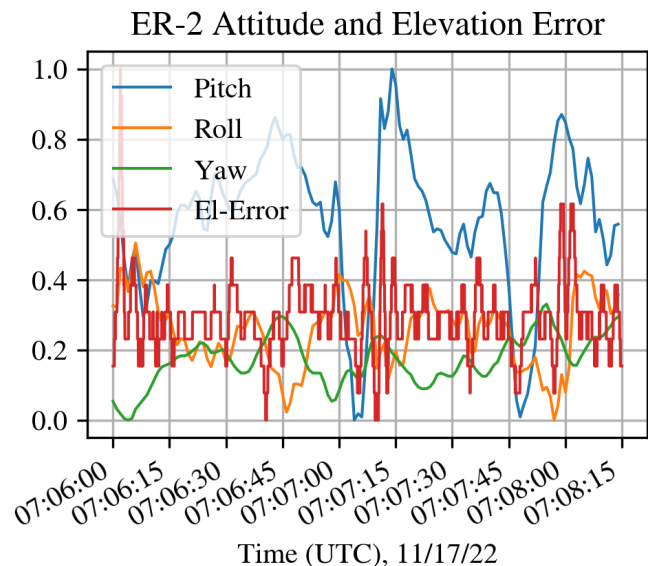


Figure 13: Elevation error dependence on the roll attitude dynamics.

## 4. PROPOSED DESIGN: HAAMR

The proposed design for air-LUSI's second-generation robotics subsystem will now be presented, shown below in Fig. 15. The High Altitude Aircraft Mounted Robotic (HAAMR) telescope mount is based on the bisecting axes design alternative, which has been shown to offer an increased FOR, improved high-frequency disturbance rejection, and reduced actuator loads. The outer gimbal is parallel to the ER-2's roll axis and controls the elevation angle of the telescope, whereas the inner gimbal controls the azimuthal angle of the telescope and is aligned with the aircraft's pitch axis when the telescope is in the zenith pointing configuration, as in Fig. 15. From the perspective of lunar measurements, viewing the Moon as near to the zenith as possible is ideal since there is less atmosphere for the incident rays to travel through.

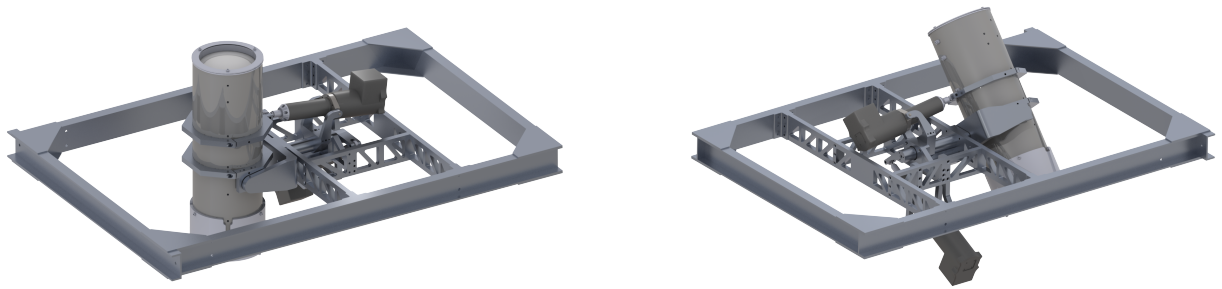


Figure 14: Preliminary design for air-LUSI's second-generation robotic telescope mount.

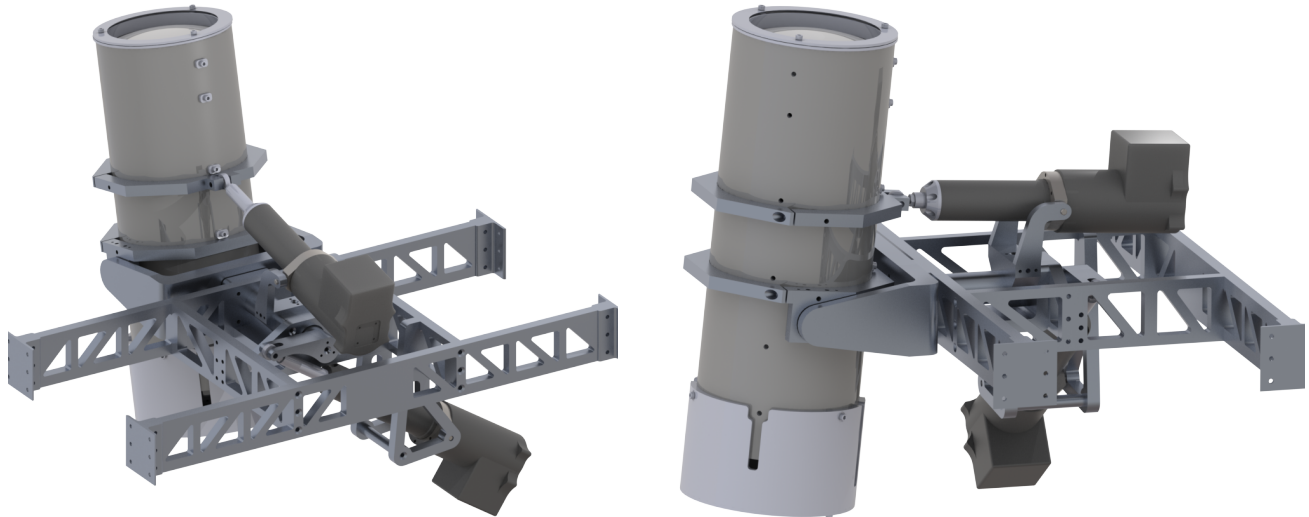


Figure 15: Close-up view of the proposed design.

The HAAMR will be entirely designed, fabricated, and tested in the ICE Lab at McMaster University. The supporting structure of HAAMR is comprised of Aluminum 2024-T3 rectangular bar, a common aerospace-grade aluminum alloy championed for its strength-to-weight ratio and fatigue strength. The frame is fixed to the AFRC mounting rack with straddled face-mounted elbow brackets. The same actuators will be employed for their ease of use, commissioning, and proven track record. The design provides  $\pm 10^\circ$  of azimuthal range of motion and allows for elevation angles from  $35^\circ - 90^\circ$  above the local horizontal. Although the instantaneous joint torque is a nonlinear function of the actuator stroke position and transmission link lengths, the proposed design can deliver continuous elevation axis torques of 9.5 – 20 Nm (min - max), and no less than 30 Nm of azimuthal torque. Compared to ARTEMIS, which could only provide continuous elevation torques from 5.5 – 10 Nm (min - max), and no less than 15 Nm to the azimuthal axis, it's reasonable to expect that the HAAMR's increased control torques, coupled with a mechanically balanced payload, will result in improved tracking performance – especially during instances of turbulence. However, this assumption can only be verified by rigorous analysis, simulation, and testing. The following section expands on the analysis and simulation efforts that will be completed in preparation for the January 2024 Operational Flight Campaign 02.

## 4.1 Next Steps and Future Work

To confirm the assumption that HAAMR will offer improved target tracking performance, the joint torques required to achieve perfect aircraft disturbance rejection must be determined through simulation. To determine the joint torques, a dynamics simulation will be performed to determine how much mass/inertia must be moved about each joint and how quickly that movement needs to occur. A joint-space trajectory defines the time history of joint angles, velocities, and acceleration that produce the desired motion. However, the desired joint trajectory must be constructed according to operationally characteristic aircraft motion profiles. The task of defining the desired joint-space trajectory can be realized through an inverse kinematics approach – from a time history of the Moon’s location relative to the aircraft and the ER-2’s attitude dynamics, an inverse kinematic model of the Moon-Aircraft-Robot system would provide the time history of joint angles, velocities, and accelerations (desired states) that keep the LOS centered on the Moon. As mentioned, this desired state trajectory can then be implemented in a dynamics simulation of the manipulator to determine the joint torques required to produce this motion.

Following validation by the simulations, the HAAMR will be fabricated and thoroughly tested in the ICE lab at McMaster University. Testing of the HAAMR according to experimentally realistic conditions is difficult, mainly for the reason that replicating the inertial loads induced on the manipulator by the ER-2 would require a dedicated testing rig. Instead, a mock telescope will be designed to impose worst-case payload weight and CG offset conditions. Lastly, the prospect of employing a hybrid visual-inertial control system will be explored, by incorporating IMU feedback in the main control loop.

## 5. CONCLUSIONS

The air-LUSI instrument is an inter-agency partnership that aims to improve the utility of the Moon as an on-orbit calibration source. Air-LUSI makes SI-traceable measurements of lunar spectral irradiance from the wing pod of a NASA ER-2 aircraft. In order to capture the data accurately, a robotic telescope mount is required to maintain the telescope’s LOS on its target, by compensating for aircraft and lunar motion.

Since 2018, the air-LUSI instrument had employed the ARTEMIS for autonomous lunar tracking on more than ten high-altitude flights. ARTEMIS’ performance was exceptional early on in its lifetime, but unfortunately, deteriorated over the years as the team pursued more aggressive lunar elevations, more frequent flights, and problems inherent to the design began to manifest operationally. ARTEMIS’ last flight occurred on 17/11/2022, in which multiple actuator failures resulted in an aborted flight and solidified the need for an upgraded robotics system.

In this paper, an overview of ARTEMIS’ historical performance in the field, along with the numerous lessons learned from those campaigns, was presented. Through extensive field experience, the air-LUSI team targeted a number of desired changes to the robotics subsystem in order to continue deploying the air-LUSI instrument in a reliable manner. The desired changes are analyzed in the context of experimental data, and a preliminary design was proposed according to the justifications. The HAAMR, poised to replace the ARTEMIS on future flight campaigns, is on track to significantly improve lunar tracking performance for the air-LUSI instrument and offer a reliable autonomous platform for high-altitude measurements. Ultimately, the HAAMR will enable the acquisition of lunar spectral measurements that aim to improve the utility of the Moon as an on-orbit calibration source, and thus improve the accuracy of remote sensing instruments responsible for monitoring the affects of global climate change.

## APPENDIX A. FULL RESOLUTION TARGET TRACKING PLOTS

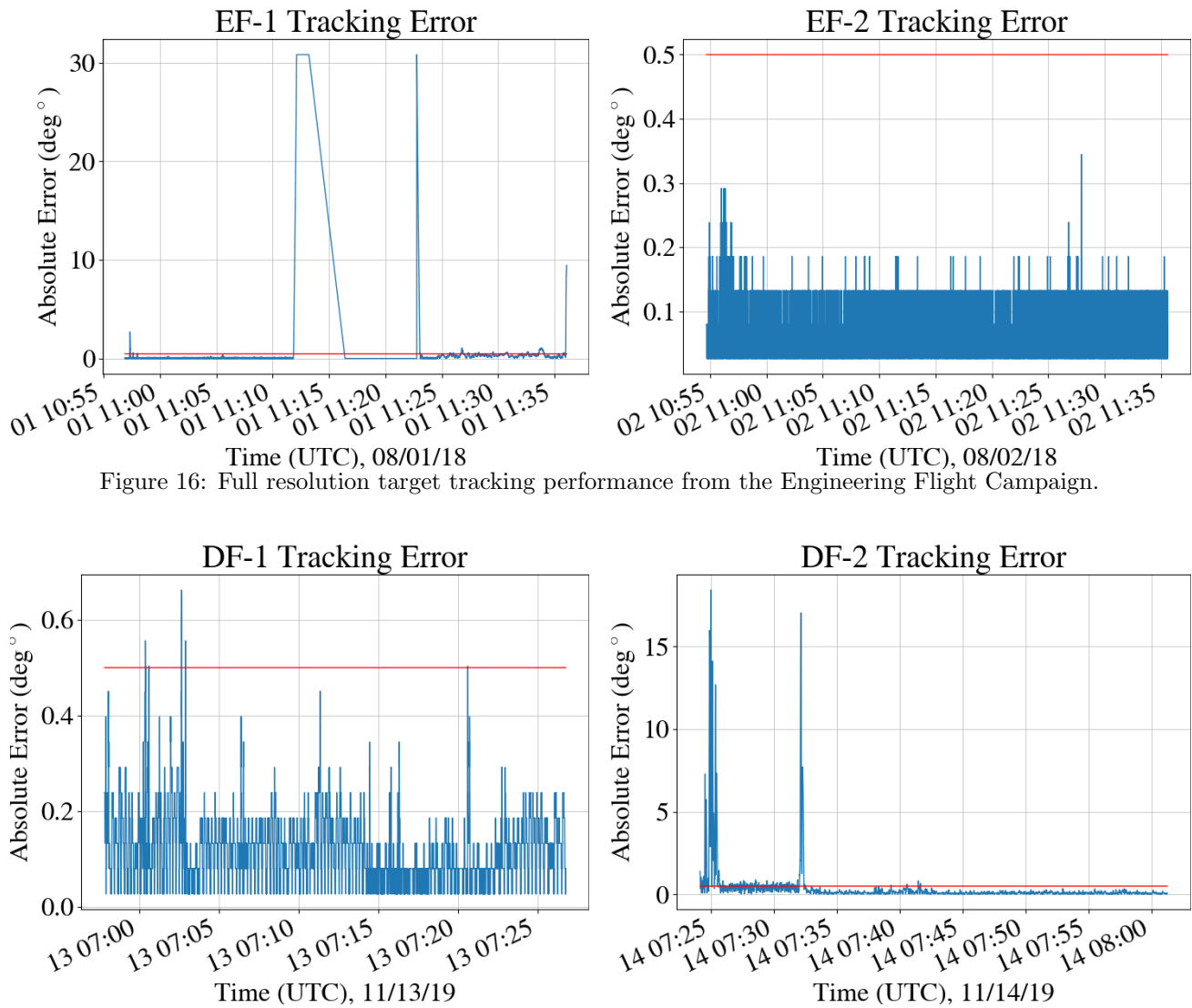


Figure 16: Full resolution target tracking performance from the Engineering Flight Campaign.

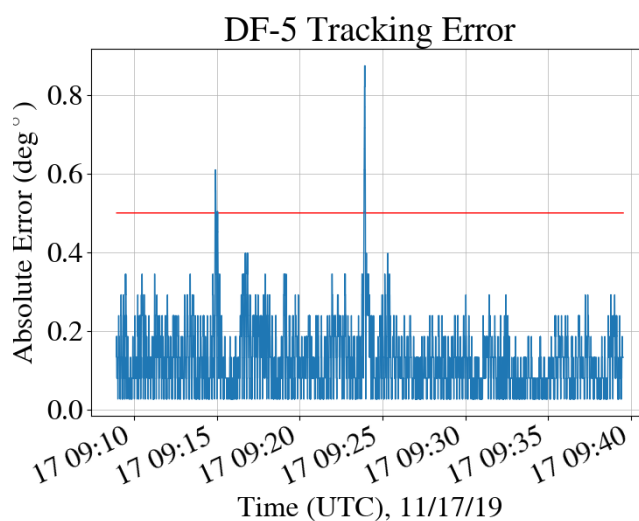
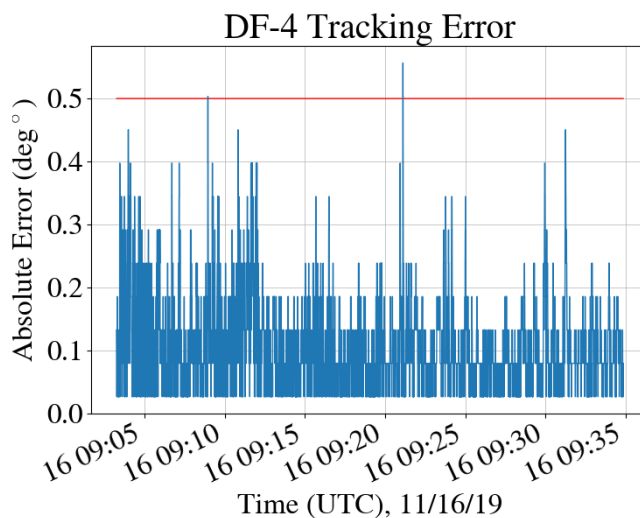
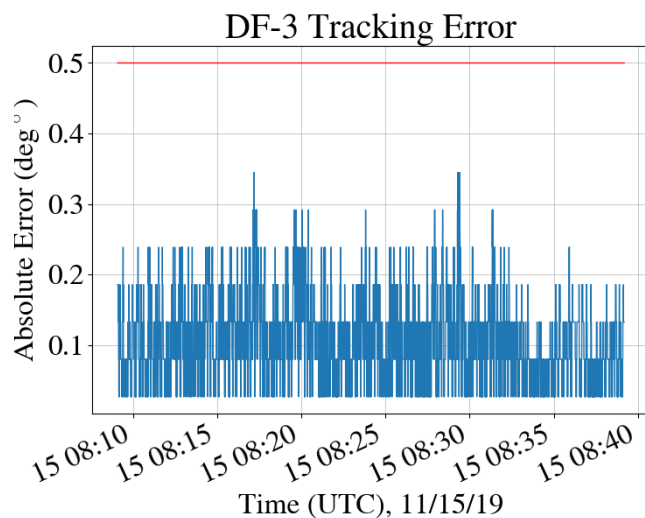
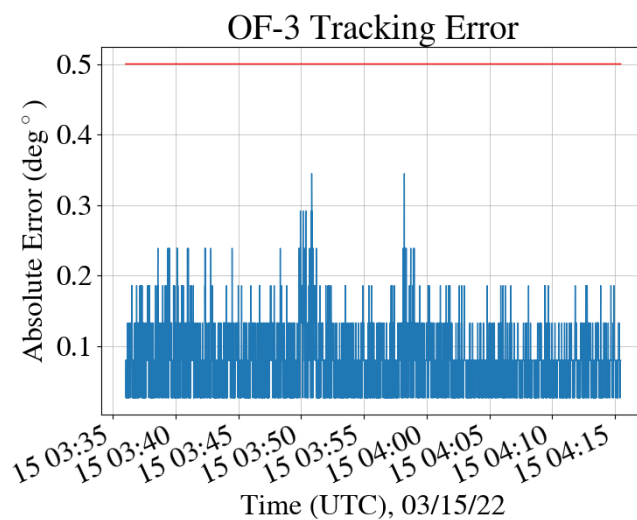
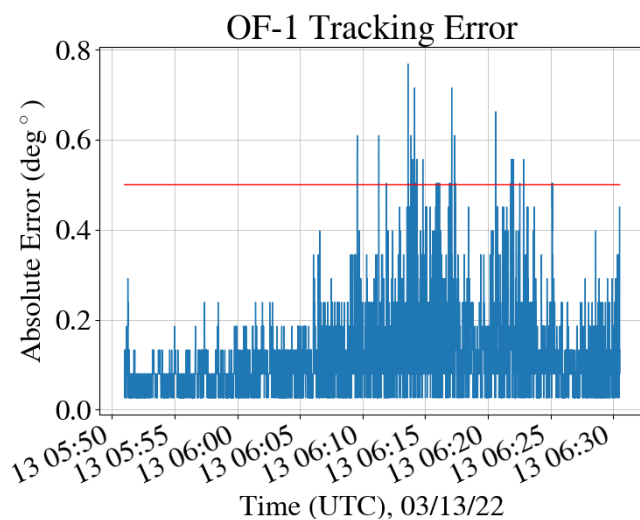


Figure 17: Full resolution target tracking data for the Demonstration Flight Campaign



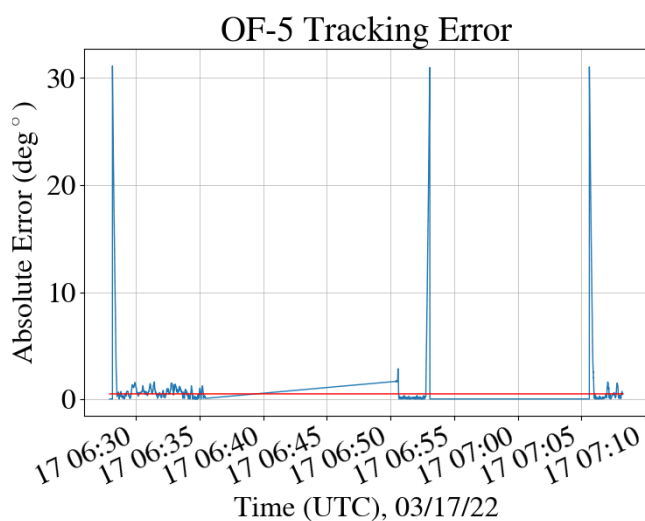
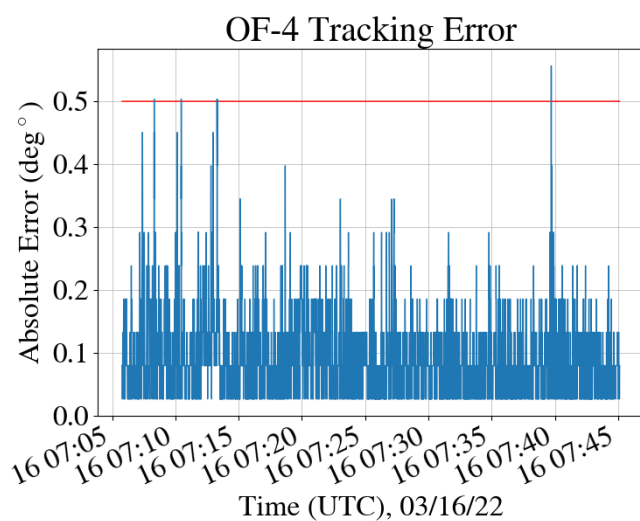


Figure 18: Full resolution target tracking plots from the Operational Flight Campaign 01.



## ACKNOWLEDGMENTS

The authors would like to thank the other members of the air-LUSI team, including: John T. Woodward, Thomas C. Stone, Steven E. Grantham, Stephen E. Maxwell, and Thomas C. Larason. We would also like to express our thanks to the staff at NASA's Armstrong Flight Research Center (AFRC) for enabling the success of this project, as well as the staff at NIST and NASA headquarters for their valuable support.

## REFERENCES

- [1] National Institute of Standards and Technology, "Satellite instrument calibration for measuring global climate change," Tech. Rep. NIST Internal Reports (NISTIRs), U.S. Department of Commerce, Washington, D.C. (2002).
- [2] Kieffer, H. H., Stone, T. C., Barnes, R. A., Bender, S. C., Jr., R. E. E., Mendenhall, J. A., and Ong, L., "On-orbit radiometric calibration over time and between spacecraft using the Moon," in [*Sensors, Systems, and Next-Generation Satellites VI*], Fujisada, H., Lurie, J. B., Aten, M. L., Weber, K., Lurie, J. B., Aten, M. L., and Weber, K., eds., **4881**, 287 – 298, International Society for Optics and Photonics, SPIE (2003).
- [3] Kieffer, H. H., "Photometric stability of the lunar surface," *Icarus* **130**(2), 323–327 (1997).
- [4] Kieffer, H. H. and Stone, T. C., "The spectral irradiance of the moon," *The Astronomical Journal* **129**, 2887 (jun 2005).
- [5] Stone, T. C., "The moon as a radiometric reference source for on-orbit sensor stability calibration," in [*2009 IEEE International Geoscience and Remote Sensing Symposium*], **5**, V–232–V–235 (2009).
- [6] Stone, T. C., Kieffer, H., Lukashin, C., and Turpie, K., "The moon as a climate-quality radiometric calibration reference," *Remote Sensing* **12**(11) (2020).
- [7] Navarro, R., "The NASA earth research-2 (ER-2) aircraft: A flying laboratory for earth science studies," Tech. Rep. NASA/TM-2007-214615, National Aeronautics and Space Administration, Edwards, California (2007).
- [8] Grantham, S. E., Turpie, K. R., Stone, T. C., Gadsden, S. A., Larason, T. C., Zarobila, C. J., Maxwell, S. E., Woodward, J. T., and Brown, S. W., "The irradiance instrument subsystem (IRIS) on the airborne lunar spectral irradiance (air-LUSI) instrument," *Measurement Science and Technology* **33** (March 2022).
- [9] Woodward, J. T., Turpie, K. R., Stone, T. C., Gadsden, S. A., Newton, A., Maxwell, S. E., Grantham, S. E., Larason, T. C., and Brown, S. W., "Measurements of absolute, SI-traceable lunar irradiance with the airborne lunar spectral irradiance (air-LUSI) instrument," *Metrologia* **59** (May 2022).
- [10] Cataford, A., *air-LUSI: The Mechanical and Control System Design of NASA's Airborne Lunar Observatory*, Master's thesis, University of Guelph (2018).
- [11] Newton, A., Cataford, A., Maxwell, S. E., Gadsden, S. A., and Turpie, K., "Air-lusi: Development of a pointing and tracking control system for lunar spectral measurements," *Acta Astronautica* **176**, 558–566 (2020).
- [12] Craig, J. J., [*Introduction to Robotics Mechanics and Control*], ch. 2, Pearson Education, Inc, 3rd ed. (2005).